COBEM 2023 27TH INTERNATIONAL CONGRESS OF MECHANICAL ENGENEERING

ABCM Brazilian Society of Mechanical Sciences and Engineering
27th ABCM International Congress of Mechanical Engineering
December 04-08, 2023, Florianópolis-SC, Brazil

COB-2023-0975
SEPARATION EFFICIENCY ANALYSIS OF A SUPERSONIC SEPARATOR NOZZLE WITH CENTRAL BODY

Thomaz Garcia Faccioli
Reinaldo Marcondes Orselli, Ph.D
Federal University of ABC, Center for Engineering, Modeling and Applied Social Sciences, Avenida dos Estados, 5001, Santo André, SP, Brazil.
thomaz.faccioli@aluno.ufabc.edu.br
reinaldo.orselli@ufabc.edu.br

Ricardo Galdino da Silva, Ph.D
Aeronautics and Space Institute, Department of Aerospace Science and Technology, Praça Marechal Eduardo Gomes, 50, São José dos Campos, SP, Brazil.
ri_galdino@yahoo.com.br

Denis Fernando Grégorio Junior, BSc
Bruno Souza Carmo, Ph.D
University of São Paulo, Escola Politécnica, Department of Mechanical Engineering, Av. Prof. Mello Moraes, 2231, São Paulo, SP, Brazil.
denis.fernando@usp.br
bruno.carmo@usp.br

Abstract. *The supersonic gas separator is a new technology that uses the processes of supersonic expansion and cyclonic separation to remove water and condensates, such as CO_2, from natural gas. The objective of this study is to perform CFD simulations with particles injection known as DPM (Discrete Phase Method) to investigate the effect of the centrifugal force on the separation efficiency of such device. For the supersonic separator geometry, the configuration is considered with central body, specially designed to increase the separation efficiency. The supersonic device is formed by a converging-diverging section in which the flow is accelerated to supersonic speed in the nozzle, followed by a diffuser where a train of shock waves occurs, and static pressure is recovered. The process of separation occurs by supersonic expansion, which decreases the gas temperature such that some components (particularly CO_2) are condensed; in turn, the liquid droplets formed are separated from the gas being conducted by centrifugation towards downstream collectors installed on the nozzle walls. Among the numerical simulations carried out, for a centrifugal acceleration of 350,000 g, the highest separation efficiency obtained was 98%.*

Keywords: *Computational Fluid Dynamics, Natural gas, Shock wave, Supersonic separator, Discrete Phase Model*

1. INTRODUCTION

As a result of the increasing global energy demand and the urgent need to mitigate the environmental consequences associated with current energy production methods, there is a growing imperative to develop innovative technological solutions. These solutions aim to minimize greenhouse gas emissions and optimize the exploration of energy sources. Therefore, natural gas has turned into a great alternative to compose the energy matrix of several countries, as, in comparison to others traditional fossil fuels, it has a lower emission of gases harmful to the environment. As one of the primary environmental objectives, the reduction of CO_2 gas emissions in the atmosphere holds significant importance, according to Silva (2010), natural gas emits about 20 to 30% less CO_2 gases less compared to fuel oil and 40 to 50% less if compared with solid fuels, such as coal.

Natural gas is essentially a mixture of hydrocarbons in gaseous form, in which the main component is methane (CH_4). Some of the other components, such as CO_2, must be removed as long as the presence of this component reduces heating value of the natural gas and it causes corrosion of the pipes (Altam *et al.*, 2017). With the aim of enhancing efficient transportation and commercialization, there is a need to create compact equipment that can purify natural gas directly at offshore platforms.

Within this context, a newly proposed technology called a supersonic separator has emerged. This innovative approach utilizes expansion processes to effectively cool and condense the heavier components, such as CO_2, allowing the liquid part to be separated from the gas by centrifugation. Regarding the challenges and demands set out above, this device has

several advantages compared to other traditional arrangement, such as membrane permeation and chemical absorption: there is no moving parts, there is no need for chemical products, it is very compact, there is no requirement for manual operation, the device is lighter and less costly, lower maintenance and, in operational terms it is energetically more efficient (Liu *et al.*, 2014) (Arinelli *et al.*, 2015).

As shown in Fig. 1, the concept of supersonic separator is composed of a Laval nozzle, a collector and a diffuser. The fluid is accelerated in the convergent section of the Laval nozzle, then, becoming supersonic in the divergent section. There, the gas expands causing a decrease in the static pressure and temperature. As such, water and some heavier hydrocarbon components are condensate in the divergent section and are carried towards the wall due to the centrifugation imposed, and finally removed through the collector.

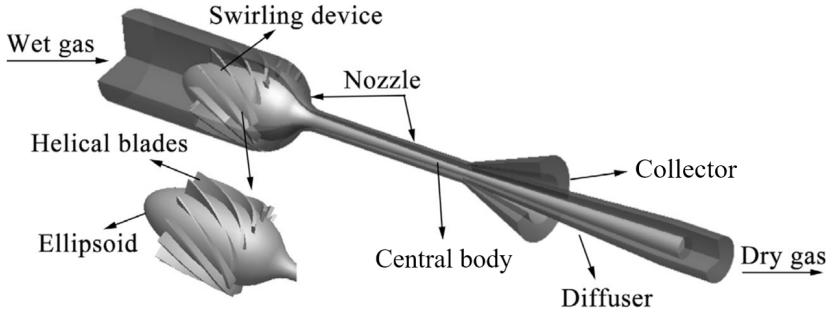

Figure 1. Structure of a supersonic separator with central body (Wen *et al.*, 2016).

As the flow in a supersonic separator has complex operating conditions with high velocity and pressure gradients coupled with formation of shock waves and consequent interactions with the boundary layer, there is a need to carry out careful studies regarding such issues, evaluating the flow behavior as well as optimizing the system. For this purpose, numerical simulations are performed to give a better understanding of the behavior of the flow in a simplified model of a supersonic separator. In addition, the capability of such numerical simulations to predict and deal with a such complex flow observed in this device is analyzed, for example, with the presence of shock wave, boundary layer interaction, flow separation and centrifugation.

Regarding the scenario set above, the objective of this work is to perform numerical simulations of the flow through an axisymmetric model representing the supersonic separator with a particular geometry based on the device developed by Twister BV, which has a central body. As illustrated in Fig. 1, the central body has the function of making the induced swirl more efficient, allowing the condensed particles to be carried towards the collector. In addition, to investigate the main characteristics of the flow through this device, the separation efficiency and its relation to the centrifugal acceleration of the flow are also studied by injecting discrete particles into the flow, representing CO_2 droplets.

2. METHODOLOGY

As above-mentioned, numerical simulations (CFD - Computational Fluid Dynamics) were carried out in order to investigate the flow behavior through the supersonic separator considering different centrifugation levels. For the numerical calculations, the commercial code Ansys Fluent was used to solve the governing equations of the fluid mechanics by means of the discretization method based on the finite volume method. The fluid was regarded as a continuum and the equations of conservation of mass, momentum and energy, described in section 2.1, were solved iteratively in the axisymmetric computational domain.

Furthermore, the pressure-based solver was employed to solve the equations, wherein the constraint of mass conservation of the velocity field is achieved by solving a pressure equation. In this algorithm, the pressure equation is derived from the continuity and the momentum equations in such a way that the velocity field, corrected by the pressure, satisfies the continuity equation (Ansys, 2022a). Besides that, for the coupling of the velocity field and pressure, the SIMPLE (Semi-Implicit Method for PressureLinked Equations) algorithm was applied in which the relationship between velocity and pressure corrections is used to impose mass conservation and to determinate the pressure field (Patankar and Spalding, 1972). Additionally, for the spatial discretization, the second-order upwind scheme was adopted for all flow variables.

Since the numerical solution of the flow through the supersonic separator was obtained through an iterative method, a convergence criterion was used. Accordingly, a residual was calculated for each iteration, and its value should decrease along the simulation as the numerical results approximates the numerical solution according to the discretized flow equations. The residual computed by Ansys Fluent's pressure-based solver is the imbalance of each discretized transport equation summed over all cells of the domain at the current iteration, scaled by the flux of the main variable at the cell center according to each equation (Ansys, 2022a). The established convergence criterion was set to at least a maximum residual value of 1e-6 for the energy equation and 1e-3 for the rest of the transport equations, as recommended for

converged simulation by Ansys (2022b). In addition to the residual convergence mentioned, the main flow parameters, including the maximum Mach number and minimum static temperature, were continuously monitored throughout the iterations, and the solution was deemed converged when significant fluctuations were no longer observed.

For the simulations, an axisymmetric domain was considered to represent the flow inside the supersonic separator. Besides that, as the flow reaches Mach number values greater than 0.3, the gas was considered as compressible. Additionally, the fluid is regarded to be pure methane and behaves like a real gas, due to the thermodynamic conditions achieved in the supersonic separator (high pressure and low temperature), which result in distinct response compared to an ideal gas. Therefore, the Redlich-Kwong real gas equation (Redlich and Kwong, 1949) was employed to predict the flow dynamics because, as demonstrated in the study by Yang *et al.* (2014), this model effectively captured the shock wave position and flow characteristics, exhibiting a strong correlation with experimental data obtained from a supersonic separator. In addition, since the aim of this work is to carry out a preliminary study of the flow through a simplified axisymmetric supersonic separator model, the condensation effects on the flow were not contemplated in the numerical simulations.

2.1 Swirling Flow

As indicated above, the flow in the supersonic separator was simulated by considering the numerical domain as axisymmetric, but still including the swirl (or circumferential) velocity, as illustrated in Fig. 2. It is important to note that while the assumption of axisymmetry implies that there are no circumferential gradients in the flow (Ansys, 2022b). The governing equations for axisymmetric swirling flow of a compressible fluid are:

Continuity equation (divergence free velocity field),

$$\frac{\partial \rho}{\partial t} + \nabla \cdot (\rho \mathbf{V}) = \frac{\partial \rho}{\partial t} + \frac{\partial}{\partial x}(\rho u) + \frac{\partial}{\partial r}(\rho v) + \frac{\rho v}{r} = 0 \tag{1}$$

Axial momentum equation,

$$\begin{aligned} &\frac{\partial}{\partial t}(\rho u) + \frac{1}{r}\frac{\partial}{\partial x}(r\rho u u) + \frac{1}{r}\frac{\partial}{\partial r}(r\rho v u) = \\ &-\frac{\partial p}{\partial x} + \frac{1}{r}\frac{\partial}{\partial x}\left[r\mu\left(2\frac{\partial u}{\partial x} - \frac{2}{3}(\nabla \cdot \mathbf{V})\right)\right] + \frac{1}{r}\frac{\partial}{\partial r}\left[r\mu\left(\frac{\partial u}{\partial r} + \frac{\partial v}{\partial x}\right)\right] \end{aligned} \tag{2}$$

Radial momentum equation,

$$\begin{aligned} &\frac{\partial}{\partial t}(\rho v) + \frac{1}{r}\frac{\partial}{\partial x}(r\rho u v) + \frac{1}{r}\frac{\partial}{\partial r}(r\rho v v) = \\ &-\frac{\partial p}{\partial r} + \rho\frac{w^2}{r} + \frac{1}{r}\frac{\partial}{\partial x}\left[r\mu\left(\frac{\partial v}{\partial x} + \frac{\partial u}{\partial r}\right)\right] + \frac{1}{r}\frac{\partial}{\partial r}\left[r\mu\left(2\frac{\partial v}{\partial r} - \frac{2}{3}(\nabla \cdot \mathbf{V})\right)\right] - 2\mu\frac{v}{r^2} + \frac{2}{3}\frac{\mu}{r}(\nabla \cdot \mathbf{V}) \end{aligned} \tag{3}$$

Circumferential momentum equation,

$$\frac{\partial}{\partial t}(\rho w) + \frac{1}{r}\frac{\partial}{\partial x}(r\rho u w) + \frac{1}{r}\frac{\partial}{\partial r}(r\rho v w) = -\frac{vw}{r} + \frac{1}{r}\frac{\partial}{\partial x}\left[r\mu\frac{\partial w}{\partial x}+\right] + \frac{1}{r^2}\frac{\partial}{\partial r}\left[r^3\mu\frac{\partial}{\partial r}\left(\frac{w}{r}\right)\right] \tag{4}$$

Energy equation,

$$\frac{\partial}{\partial t}(\rho e_t) + \nabla \cdot [\mathbf{V}(\rho e_t + p)] = \nabla \cdot [k\nabla T + (\bar{\bar{\tau}} \cdot \mathbf{V})] \tag{5}$$

where t, ρ and p are time, fluid density and pressure, u, v and w are axial, radial and circumferential velocity components, respectively, $\mathbf{V}$ is the velocity vector and r and x are the radial and axial component, respectively. Regarding the energy conservation equation, T, e_t, $\bar{\bar{\tau}}$ and k are temperature, energy per unit of mass, shear stress tensor and thermal conductivity, respectively. The above axisymmetric swirling flow model, which is implemented in the Fluent code, is used for the present computations together with the k-ω SST turbulence model discussed below.

In order to describe the velocity distribution in the circumferential direction that would be generated by the static vane geometry, a parabolic profile was employed in the inlet velocity boundary condition. Therefore, the circumferential velocity magnitude at the inlet, established by the pressure boundary conditions, vary parabolically along the domain inlet with zero velocity on the separator walls and central body. In this study, the velocity components were determined by taking the average velocity within each mesh cell of the inlet section, with the weighting based on the cell's area. Then, the inlet fluid velocity was set based on the vector sum of average circumferential and axial velocities. The swirl level was specified as the angle θ between the flow velocity direction and the axial component, representing the vane angle. Thus, the angle θ can be computed by $\arctan(u/w)$. Accordingly, considering the velocity average constant determined by the boundary conditions, an increment of the angle θ increases the circumferential velocity.

In addition, to evaluate the centrifugation caused by a certain angle θ, the centrifugal acceleration through the supersonic separator was determined by $a = w^2/r$.

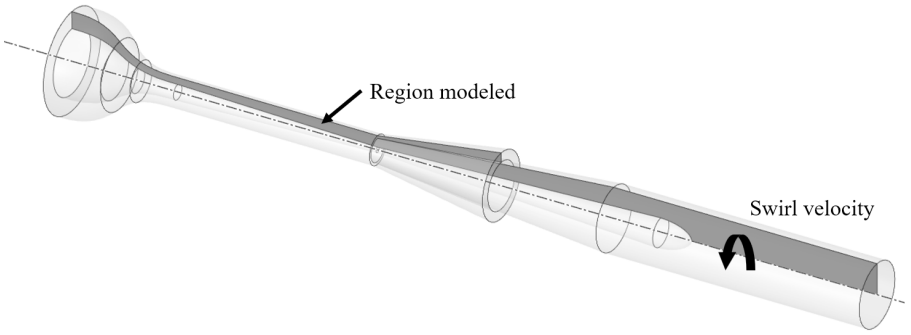

Figure 2. Computational domain of the axisymmetric model of the supersonic separator with central body used for the simulations.

2.2 Turbulence Modeling

Due to the elevated velocity as supersonic with the occurrence of shock waves, the flow is characterized as highly turbulent. Thus, in order to deal with the highly turbulent flow characterized by a broader range of scales in terms of variations frequencies and eddies sizes, the RANS (Reynolds Averaged Navier-Stokes) equations approach is used. The RANS equations are based on the time-averaged Navier-Stokes equations, whereby the turbulent flow is characterized in terms of the mean value of flow property and some empirical or at least semi-empirical information on the turbulence structure and its relation to the averaged flow (Hirsch, 2007). The application of the time-averaged Navier-Stokes equations results in a non-linear term dependent on the fluctuating part of the flow velocities, which is known as the Reynolds stress tensor. In order to close the RANS equations with the unknown Reynolds stress tensor, the Boussinesq hypothesis is used to relate the fluctuating terms with the mean flow (Versteeg and Malalasekera, 2007). Some proposed models based on the Boussinesq hypothesis involves additional variables to statistically quantify the fluctuating component, such as the turbulence kinetic energy (k) and its dissipation represented by "Epsilon" (ϵ) or "Omega" (ω), the specific rate of dissipation of turbulence. For this work, the Shear-Stress Transport (SST) k-ω model (Menter, 1994) is used, as it is more accurate and reliable for pressure gradient flows and transonic shock waves (Ansys, 2022a). The above-mentioned turbulence model SST k-ω is a hybrid model as based on the combination of two basic models, known as the k-ϵ model and the k-ω model. In the near-wall region, this hybrid model uses a transformation of k-ϵ model into a standard k-ω and the standard k-ϵ model in the fully turbulent region far from the wall (Versteeg and Malalasekera, 2007).

2.3 Geometry and Mesh

The geometry considered for the numerical simulations, shown in Fig. 3, is based on the design developed by Twister BV and the published works of Cao and Yang (2015) and Wen *et al.* (2011b), who studied the flow behavior of the supersonic separator. This geometry has a particular feature of a central body designed to improve the centrifugation process, also providing more stability of the flow avoiding separation or decrease of flow velocity. The ellipsoidal shape and static vanes at the upstream side of the central body were not considered for the simulation. The upstream static vanes positioned before the nozzle are designed to change the direction of flow velocity, thereby inducing centrifugation. Since the domain is considered as axisymmetric, the static vanes are not considered for the simulation and the direction of the flow was imposed as an inlet boundary condition. The tunnel bounded by the wall and the central body forms the convergent-divergent nozzle and diffuser. As observed in Fig. 3, just downstream the throat there is the divergent section, also known as cyclonic separation, where the flow is supersonic, that ends at the division of the flow between the collector entrance and the diffuser section.

The diameter of the wall and central body in the convergent section of the Laval nozzle, where the fluid is accelerated up to sonic speed at the throat, are described by

$$\begin{cases} \dfrac{D - D_{th}}{D_{in} - D_{th}} = 1 - \dfrac{1}{X_m^2}\left(\dfrac{x}{L_{conv}}\right)^3, & \left(\dfrac{x}{L_{conv}} \leq X_m\right) \\ \dfrac{D - D_{th}}{D_{in} - D_{th}} = \dfrac{1}{(1 - X_m)^2}\left(1 - \dfrac{x}{L_{conv}}\right)^3, & \left(\dfrac{x}{L_{conv}} \leq X_m\right) \end{cases} \tag{6}$$

where D_{in}, D_{th} and L_{conv} are the inlet diameter, the throat diameter and the convergent section length, respectively. X_m is the relative coordinate of this convergent curve set 0.45 and D is the diameter for a certain value of x. Table 1 shows the main proportions of the supersonic separator geometry used in this study, where A_{inlet}, A_{throat}, $A_{div,out}$, $A_{coll,in}$ being the area sections of the separator inlet, throat, divergent outlet and collector inlet, respectively, and L_{div} = 323 mm, L_{coll}

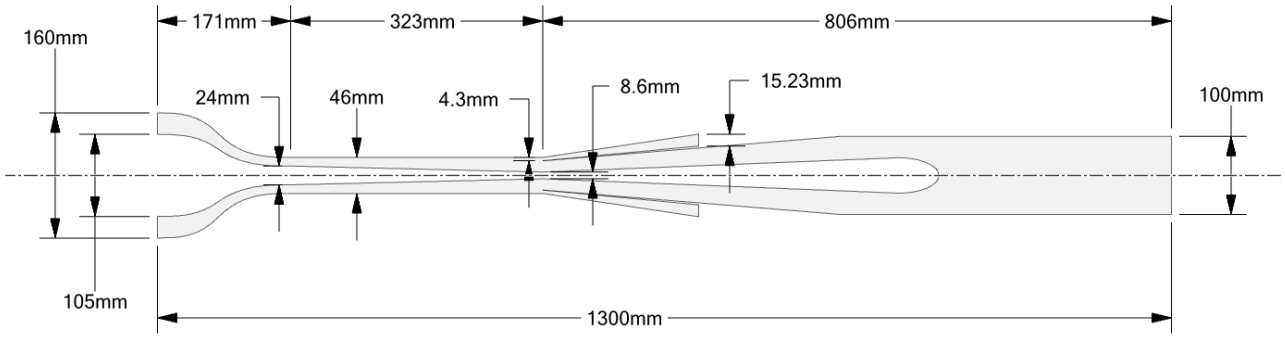

Figure 3. Cross-section of the axisymmetric supersonic separator design considered.

= 200 mm and L_{total}=1300 mm being the length of the divergent section, collector and total of the supersonic separator, respectively.

Table 1. Main proportions of the supersonic separator geometry.

Dimension	**Value**
A_{inlet}/A_{throat}	9.43
$A_{div,out}/A_{throat}$	1.32
$A_{coll,in}/A_{div,out}$	0.35
L_{coll}/L_{total}	0.15
L_{div}/L_{total}	0.25

For the numerical simulations, the structured mesh shown in Fig. 4 was generated with a total of 55500 cells. The mesh was refined in the beginning of the diffuser and collector sections to capture the high velocity gradients verified in these regions as a consequence of the shock waves.

The y^+ is the non-dimensional distance of the first cell adjacent to the wall and was used as a domain discretization parameter to identify in which region of the boundary layer the centroid of the first mesh cell is located, viscous sublayer, buffer layer log-law layer. The mesh employed for simulating the flow within the supersonic separator was created with y^+ values ranging from 30 to 350, and as such, a log-law wall function is applied to solve the flow velocity gradients of the boundary layer.

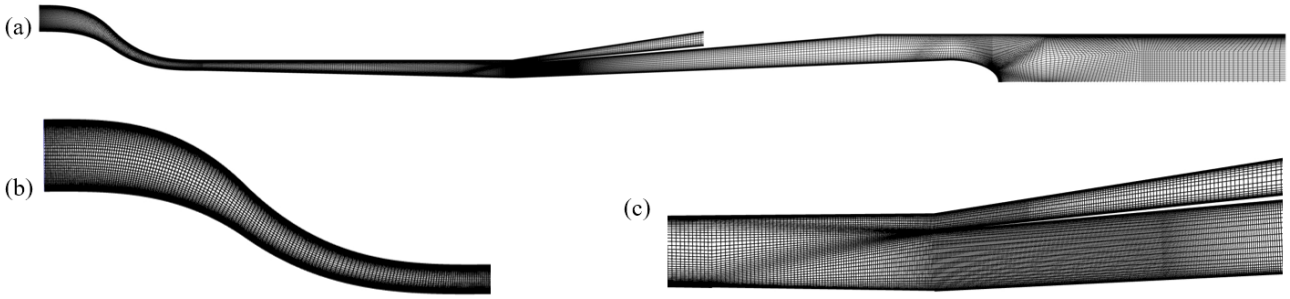

Figure 4. Computational mesh of the axisymmetric model of the supersonic separator with central body used for the simulations (a), expanded view of the convergent section (b), and expanded view of the shock waves region (c).

2.4 Discrete Phase Model

As mentioned above, the effect of condensation was not considered in this work, nonetheless, the trajectory of the droplets eventually formed from condensation in the flow can be studied. Thus, the Discrete Phase Model (DPM) is used to investigate the trajectory of droplets injected at a certain point in the flow forced into the collector by centrifugation. The DPM is a multiphase model in which the fluid phase is taken as continuous and a second discrete phase is simulated in a Lagrangian reference system. In this study, the discrete phase consists of inert spherical particles dispersed in the continuous phase representing the CO_2 liquid droplets condensed in the supersonic separator. The trajectory of these particles is computed individually and are determined by considering particle inertia and hydrodynamic drag due to its interaction with the continuous phase. Furthermore, in this modeling, the displaced fluid volume and particle collision

are neglected, as these effects are assumed to be insignificant for a discrete phase mass flow rate less than 10% of that of the fluid (Ansys, 2022b). In this work, the particle trajectory was simulated in steady state, and we considered that the fluid phase is not affected by the discrete phase. Additionally, the effect of evaporation of the liquid droplets was ignored in the simulations and the initial velocity of the liquid particles was equal to the gas speed, obtained by the numerical calculation.

In a preliminary scenario, the particles were injected in points equally spaced along a line positioned through the nozzle throat cross-section. The particle density was considered constant with a value of the CO_2 density in the liquid phase at 236 K and saturation pressure, 1101 kg/m^3 (ToolBox, 2017). Besides that, in order to simulate the size distribution of droplets formed during condensation in the supersonic separator, the Rosin-Rammler method (Rosin and Rammler, 1933) is used to define the diameters of the particles injected. The diameter range was divided into discrete intervals and the mass fraction of droplets with diameter larger than d, Y_d, was given by

$$Y_d = e^{-(d/\bar{d})^n} \tag{7}$$

where $\bar{d}$ is the mean diameter and n is the spread parameter. The parameters used in this study, presented in Table 2, are based on the work of Wen *et al.* (2011a), who studied the separation efficiency by means of DPM analysis and compared it with experimental findings, revealing a significant level of agreement.

Table 2. Parameters of the Rosin-Rammler particle diameter distribution method.

Parameter	**Value**
Minimum diameter	0.1 μm
Maximum diameter	4 μm
Mean diameter	1.4 μm
Spread parameter	1.62
Number of diameters	50

In order to evaluate the separation capacity of the supersonic separator, the separation efficiency for a given particle injection is defined as the ratio between the sum of the mass of all particles that are conducted within the collector and the total mass of injected particles.

2.5 Boundary Conditions

The parameters imposed in this study were based on the typical working conditions of the supersonic separator available in the literature, such as Wen *et al.* (2011a). The total pressure and temperature imposed at the inlet are 40 bar and 300 K, respectively. The static pressure at collector and nozzle outlets were set in such a way that the shock waves in the supersonic separator occur at the upstream region of the diffuser and collector to ensure that gas at the upstream of the collector inlet is in a thermodynamic condition that leads the heavier components to condense (the phase diagram of CO_2 may provide the thermodynamic condition, supposing in a thermodynamic equilibrium state). For this, the static pressure at the collector and diffuser outlets imposed for the numerical simulations with no swirl imposed were 24 bar and 26 bar, respectively. Since increasing centrifugation in the flow moves the shock wave upstream due to the conversion of axial to swirl velocity, the static pressure of the diffuser and collector outlet is reduced to 16 bar and 18 bar, respectively, while the θ angle was increased to 58°. The static temperature of both outlet sections was 300 K as well as at the inlet section. For the turbulence parameters, the turbulence intensity and the viscosity ratio were set as 0.035 and 1 for the inlet, and 0.042 and 4 for the outlet, respectively (Wen *et al.*, 2011b). Adiabatic no-slip wall was adopted at the separator wall and central body and symmetry condition for the axis line.

3. RESULTS AND DISCUSSION

Regarding the numerical set-up as aforementioned in section 2, numerical simulations were carried out to obtain the flow field solution along the supersonic nozzle. In the initial simulations, no swirl was considered in order to observe the primary characteristics of the flow through the supersonic separator. Figure 5 shows the Mach number static pressure and static temperature field in the supersonic separator, respectively. It can be seen from the figures that the flow reaches Mach 1 at the throat and is accelerated to supersonic velocity in the separation section, reaching the maximum value of Mach 1.8. As a result, the static pressure and temperature decrease up to 10 bar and 210 K in this region, which create a condition for the condensation of water and heavy components, such as CO_2. Additionally, it is observed that the shock waves are strong enough to cause flow separation, the shock bifurcates and one or more shocks appear downstream of the bifurcated shock (Matsuo *et al.*, 1999), which leads to a shock-train topology.

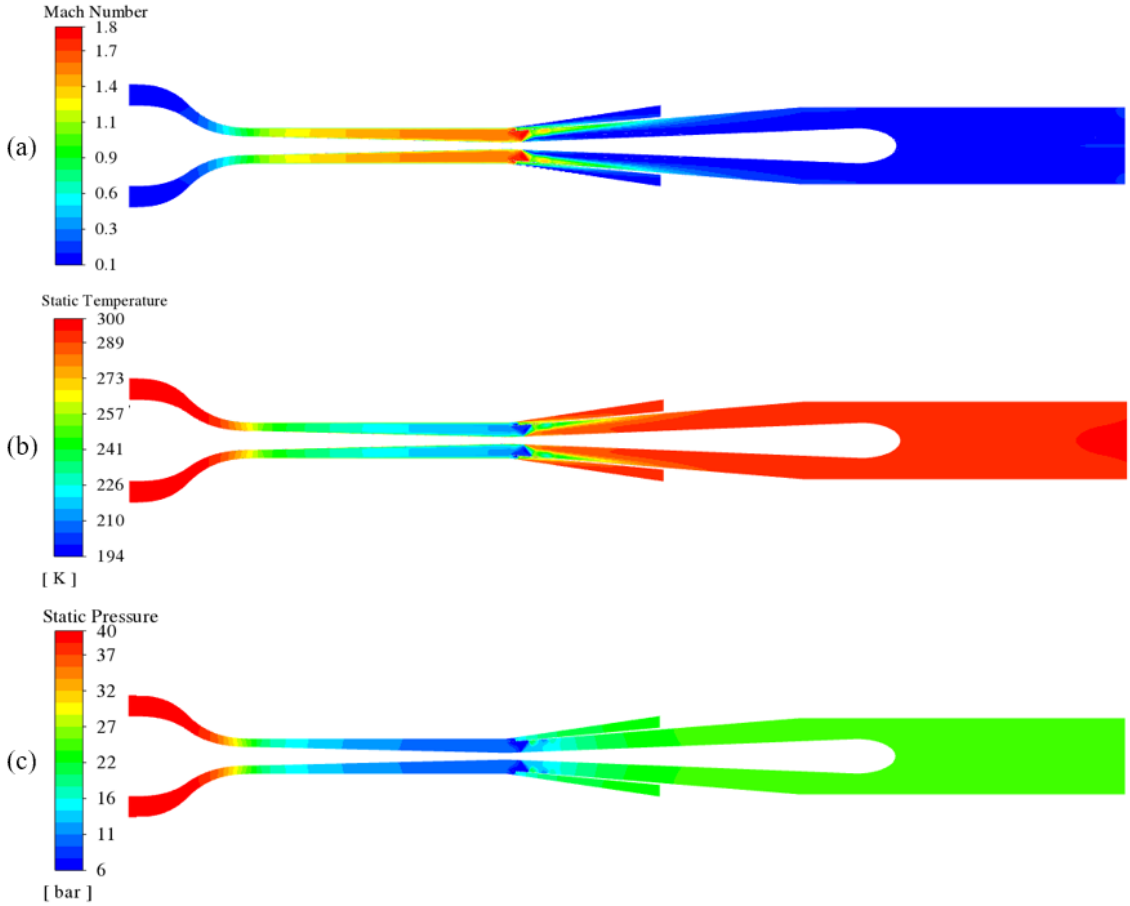

Figure 5. Simulation contour results of: (a) Mach number; (b) static pressure; (c) static temperature.

To verify that the numerical solution exhibits variation associated with mesh refinement in the domain, a mesh independence study was conducted. The purpose of the mesh independence study is to investigate the variation in the obtained solution with the mesh refinement, expecting convergence to a unique solution as the mesh is constructed of smaller volumes (or cells). Thus, the flow in the supersonic separator was simulated using three meshes: a coarse mesh (27,707 volumes), an intermediate mesh (55,550 volumes), and a fine mesh (110,362 volumes). As a reference example of the refinement mesh influence on the numerical results, Fig .6 show the variation of the static temperature along the flow centerline, there are no significant differences discernible among the three obtained solutions. It can be seen that the most pronounced difference in the results lies in the region of the shock wave due to its very fine region (the shock thickness is usually on the order of a few molecular mean free paths).

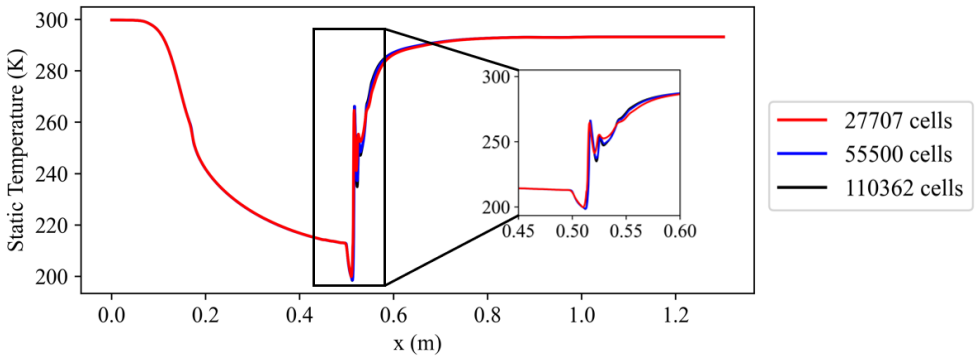

Figure 6. Static temperature values along the centerline of the flow through the supersonic gas separator with three different mesh refinements, 27707, 55550 and 110362 volumes.

3.1 Swirling Flow

Considering the configuration pointed out in section 2, simulations of the flow of the supersonic separator were performed with variation of the θ until the maximum centrifugal acceleration verified was on the order of 300,000 g, a value defined in the literature (Brouwer and Epsom, 2003) as sufficient to achieve an adequate separation rate of the higher density components of the natural gas. Furthermore, as explained in section 2.5, it is necessary to reduce the static pressure at the domain outputs to maintain the shock waves in the same position with the increase of centrifugation, thus, the static pressure at the collector and diffuser outputs were, respectively, 22 and 24 bar for $\theta = 26°$ and 20 and 22 bar for $\theta = 42°$. From Fig. 7, illustrating the centrifugal acceleration field in the supersonic separator at an angle of $\theta = 58°$, it can be noted that centrifugal acceleration increases in the divergent section up to a maximum value of 350,000 g upstream of the shock wave.

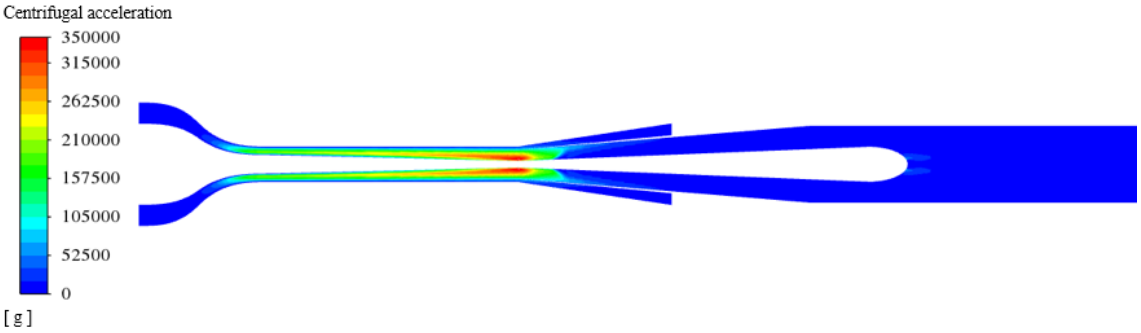

Figure 7. Centrifugal acceleration field in the supersonic separator for $\theta = 58°$.

Moreover, in order to investigate the effect of varying the angle of the inlet velocity on the centrifugal acceleration seen in the separator, Fig. 9(a) displays the maximum centrifugal acceleration obtained throughout the simulations with varying θ (see below section 3.2). It is verified that the centrifugal acceleration rises with an increase in the angle, as expected, and, for the θ angle range simulated, the maximum centrifugal acceleration of 350,000 g was achieved for $\theta = 58°$.

3.2 DPM simulation

Following the modeling described above, additional simulations were carried out considering the use of DPM. As such, the liquid particle trajectories may be tracked, enabling the evaluation of the separation efficiency in terms of particles being captured by the collector. As expected, the liquid particles injected move towards the separator wall as a result of the combined effects of the drag force and the centrifugal force. As an example, Fig. 8 illustrates solid lines inside the supersonic separator that represents the particles track injected in a single point placed in the inner region. It is noticed that most of the droplets were carried to the collector and then removed from the main flow through the supersonic device.

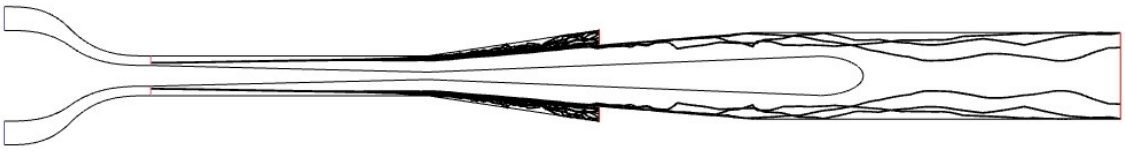

Figure 8. Trajectory of particles injected at a single point.

Considering that, for the development of the supersonic separator, it is necessary to have knowledge of the angles of the static vanes that generate the required centrifugation for achieving adequate device efficiency, Figure 9(b) illustrates the relationship between maximum centrifugal acceleration and separation efficiency for the cases evaluated in the previous section. It can be seen that the separation efficiency rises with increasing centrifugation in the flow until the maximum value of approximately 98% for 250,000 g, where above it the efficiency levels are stabilized.

With the aim of investigating the influence of particle size on separation efficiency, Fig.9(c) shows the separation efficiency of the supersonic separator considering the injection of different droplet diameters in the swirling flow with maximum centrifugal acceleration of 350,000 g. From the plot, it is noticed that, when the droplet size was 0.01 µm, the separation efficiency of the supersonic separator was 30%, approximately, and for a droplet diameter of 3 µm, the separation efficiency was 99%. This is due to the fact that when the particle's diameter of CO_2, and hence its mass, is small, the centrifugal force is not strong enough to carry the droplets to the separator wall, eventually captured by the collector. In the other hand, when the CO_2 droplet diameter grows, supposing either by condensation of the CO_2 present

in the gas phase or by agglutination, the centrifugal force plays a leading role and the droplets are carried onto the walls and collected. This effect can be explained by the fact that the value of centrifugal force experienced by a given particle is the product of its mass and the centrifugal acceleration induced by the flow, so that heavier particles can be directed towards the walls more easily. It is important to note that the simulations performed in this study did not take into account condensation or droplet size growth in the flow.

Finally, as the condensation phenomenon is not considered in the simulations, the exact region where droplet nucleation and formation of the liquid phase of the natural gas components occurs is not known. Instead, as discussed above, it is known that the flow in the divergent section of the nozzle presents the thermodynamic condition that promotes this phenomenon. Therefore, in order to investigate the effect of varying the droplet formation position on separation efficiency, DPM analyses were carried out considering different particle injection positions. Figure 9(d) shows the graph of separation efficiency as a function of position for injections made along the diverging section, where the nozzle throat is taken as the initial position and L_{div} is the divergent section length. In line with expectations, there is a reduction in efficiency as the particle injection position approaches the collector inlet. This can be attributed to the fact that as the distance between the particle injection position and the collector inlet is reduced, the particles have less length to be carried to the wall by the centrifugal force exerted by the flow. As previous results demonstrate, when particles are injected at the throat region, separation efficiency is close to 98%. However, when the injection position approaches the collector inlet, efficiency drops to 30%, with the majority of particles being collected near the collector inlet and following an approximately axial trajectory. These results demonstrate that, for the centrifugal acceleration of 350,000 g and the supersonic separator geometry considered in this study, it is necessary for CO_2 droplets to be formed at least 300 mm from the collector inlet to achieve a separation efficiency on the order of 98%.

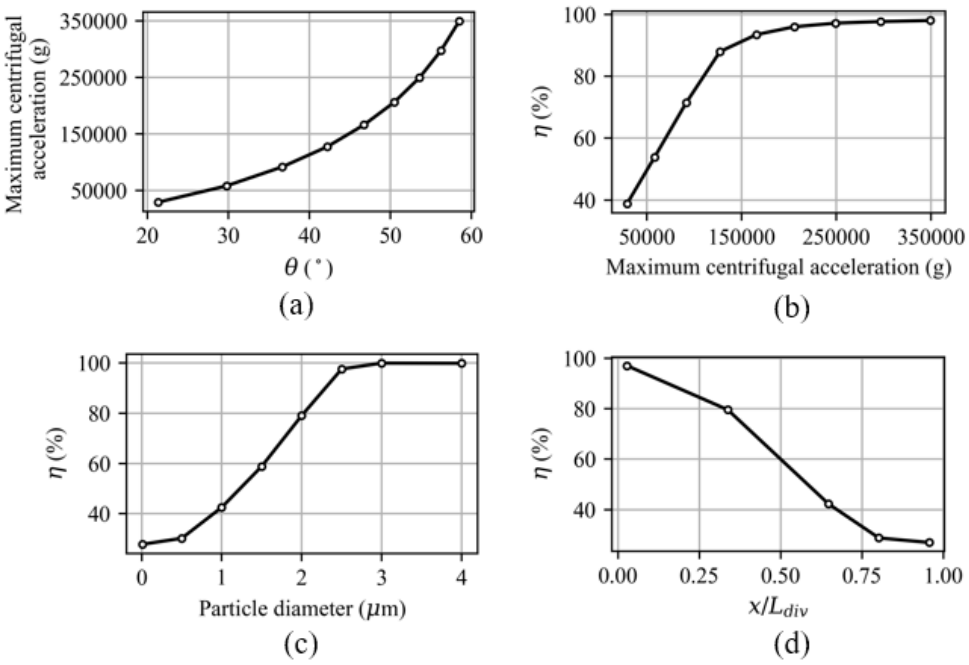

Figure 9. (a) Correlation between the angle of the inlet velocity and the centrifugal acceleration of the supersonic separator; (b) Effect of centrifugal acceleration on the separation efficiency; (c) Impact of particle diameter on separation efficiency in the 350,000 g centrifugal acceleration scenario; (d) Effect of injection position on the separation efficiency.

4. CONCLUSION

In this work, a numerical investigation of the flow behavior in a supersonic separator with central body was conducted. The flow domain was considered axisymmetric. The simulations performed considering no swirl show that the nozzle geometry and boundary conditions used in the simulations are capable of promoting the thermodynamic condition that leads to the condensation of CO_2. Moreover, the relationship between the θ angle and the maximum centrifugal acceleration in the flow was analyzed by means of the variation of the tangential component of the inlet velocity. By employing DPM simulations, we verified that, for the separator considered in this work, the maximum separation efficiency was 98%, and it was achieved when the maximum centrifugal acceleration was 250,000 g with θ = 54 °, approximately. In addition, it has also been shown that particle diameter has a significant impact on separation efficiency due to the increased centrifugal force applied to the droplets, demonstrating that, for the conditions analyzed, particles of 3 μm injected into the throat have a separation efficiency of 99%. Ultimately, as the condensation phenomenon is not considered in the simulations, DPM

analyses were carried out considering different particle injection positions. These results show that, for the centrifugal acceleration of 350,000 g and the supersonic separator geometry considered in this study, it is necessary for CO_2 droplets to be formed at least 300 mm from the collector inlet to achieve a separation efficiency on the order of 98%.

5. ACKNOWLEDGEMENTS

We gratefully acknowledge support of the RCGI – Research Centre for Gas Innovation, hosted by the University of São Paulo (USP) and sponsored by FAPESP – São Paulo Research Foundation (2014/50279-4) and Shell Brasil, and the strategic importance of the support given by ANP (Brazil's National Oil, Natural Gas and Biofuels Agency) through the R&D levy regulation. B. S. Carmo thanks the Brazilian National Council for Scientific and Technological Development (CNPq) for the financial support in the form of a productivity grant, number 314221/2021-2.

6. REFERENCES

Altam, R., Lemma, T. and Juffar, S., 2017. "Trends in supersonic separator design development". *Symposium on Energy Systems*, Vol. 131.

Ansys, 2022a. *Ansys Fluent Theory Guide*. ANSYS, Inc, Canonsburg, PA.

Ansys, 2022b. *Ansys Fluent Users Guide*. ANSYS, Inc, Canonsburg, PA.

Arinelli, L., Medeiros, J. and Araújo, O., 2015. "Performance analysis and comparison of membrane permeation versus supersonic separator for co2". *Offshore technology conference*.

Brouwer, J. and Epsom, H., 2003. "Twister supersonic gas conditioning for unmanned platforms and subsea gas processing". *Offshore Europe held in Aberdeen*.

Cao, X. and Yang, W., 2015. ""the dehydration performance evaluation of a new supersonic swirling separator". *Journal of Natural Gas Science and Engineering*.

Hirsch, C., 2007. *Numerical Computation of Internal and External Flows*. Butterworth-Heinemann, Burlington, MA.

Liu, X., Liu, Z. and Li, Y., 2014. "Investigation on separation efficiency in supersonic separator with gas-droplet flow based on dpm approach". *Separation Science and Technology*, Vol. 49, pp. 2603–2612.

Matsuo, K., Miyazato, Y. and Kim, H., 1999. "Shock train and pseudo-shock phenomena in internal gas flows". *Progress in Aerospace Sciences*, Vol. 35, pp. 33–100.

Menter, F., 1994. "Two-equation eddy-viscosity turbulence models for engineering applications". *AIAA Journal*, Vol. 21, pp. 1598–1605.

Patankar, S.V. and Spalding, D.B., 1972. "A calculation procedure for heat, mass and momentum transfer in three-dimensional parabolic flows". *Int. J. Heat Mass Transfer*, Vol. 17, p. 1787.

Redlich, O. and Kwong, J.N.S., 1949. "On the thermodynamics of solutions. an equation of state. fugacities of gaseous solutions". *Chemical Rev*, Vol. 44.

Rosin, P. and Rammler, E., 1933. "The law governing the fineness of powdered coal". *Journal of the Institute Fuel*, Vol. 7, p. 29–36.

Silva, I.D., 2010. "Natural gas: its use in electric power generation in brazil (in portuguese)". *Magazine for the Petrobras and IF Fluminense university project*, Vol. 1, pp. 103–107.

ToolBox, T.E., 2017. "Carbon dioxide - thermophysical properties". Available at: https://www.engineeringtoolbox.com/CO2-carbon-dioxide-properties-d_2017.html. Accessed 26 June 2023.

Versteeg, H.K. and Malalasekera, W., 2007. *An Introduction to Computational Fluid Dynamics - The Finite Volume Method*. Pearson Education Limited.

Wen, C., Cao, X., Yang, Y. and Zhang, J., 2011a. "Evaluation of natural gas dehydration in supersonic swirling separators applying the discrete particle method". *Advanced Powder Technology*, Vol. 23, p. 228–233.

Wen, C., Cao, X., Yang, Y. and Zhang, J., 2011b. "Swirling effects on the performance of supersonic separators for natural gas separation". *Chemical Engineering Technology*.

Wen, C., Li, A., Walther, J.H. and Yang, Y., 2016. "Effect of swirling device on flow behavior in a supersonic separator for natural gas dehydration". *Separation and Purification Technology*.

Yang, Y., Wen, C., Wang, S. and Feng, Y., 2014. "Numerical simulation of real gas flows in natural gas supersonic separation processing". *Journal of Natural Gas Science and Engineering*.

7. RESPONSIBILITY NOTICE

The authors are solely responsible for the printed material included in this paper.